Published in final edited form as:
Chemphyschem. 2014 October 6; 15(14): 2951–2958. doi:10.1002/cphc.201402398.

Theoretical Modeling of Low Energy Electronic Absorption Bands in Reduced Cobaloximes

Anirban Bhattacharjee[a], **Murielle Chavarot-Kerlidou**[b], **Jillian L. Dempsey**[c,d], **Harry B. Gray**[c], **Etsuko Fujita**[e], **James T. Muckerman**[e], **Marc Fontecave**[b,f], **Vincent Artero**[b], **Guilherme M. Arantes**[g], and **Martin J. Field**[a,*]

[(a)]Dynamo Team, DYNAMOP Group, UMR 5075, Université Grenoble 1, CNRS, CEA, Institut de Biologie Structurale — Jean-Pierre Ebel, 71 Avenue des Martyrs, CS 10090, 38044 Grenoble Cedex 9, France

[(b)]Laboratoire de Chimie et Biologie des Métaux, UMR 5249, Université Grenoble 1, CNRS, CEA, DSV/iRTSV, CEA-Grenoble, 17 rue des Martyrs F-38054 Grenoble Cedex 9, France

[(c)]Beckman Institute, California Institute of Technology, 1200 E. California Blvd., Pasadena, California 91125, USA

[(d)]Department of Chemistry, University of North Carolina at Chapel Hill, Chapel Hill, NC 27599-3290, USA

[(e)]Chemistry Department, Brookhaven National Laboratory, Upton, NY 11973-5000, USA

[(f)]Collège de France, 11 place Marcellin-Berthelot, 75005 Paris, France

[(g)]Departamento de Bioquímica, Instituto de Química, Universidade de São Paulo Av. Lineu Prestes 748, 05508-900, São Paulo, SP, Brazil

Abstract

The reduced Co(I) states of cobaloximes are powerful nucleophiles that play an important role in the hydrogen-evolving catalytic activity of these species. In this work we have analyzed the low energy electronic absorption bands of two cobaloxime systems experimentally and using a variety of density functional theory and molecular orbital *ab initio* quantum chemical approaches. Overall we find a reasonable qualitative understanding of the electronic excitation spectra of these compounds but show that obtaining quantitative results remains a challenging task.

Keywords

Cobaloxime complexes; H_2 evolving catalysts; theoretical electronic spectra; vitamin B_{12} mimics

2 Introduction

Cobaloximes are pseudo-macrocyclic bis(dialkylglyoximato) cobalt complexes, first developed in the seventies as vitamin B_{12} mimics. This family of complexes has become of

*martin.field@ibs.fr.

Europe PMC Funders Author Manuscripts

renewed interest in the past few years, following reports in 2005 [1, 2] and 2007 [3, 4, 5] of their promising hydrogen-evolving catalytic capability. Today, cobaloximes, and the related diimine-dioxime cobalt complexes [6, 7, 8, 9], are recognized as some of the most efficient molecular catalysts for electro- and photo-catalytic hydrogen evolution [10, 11, 12]. These compounds are known to be powerful nucleophiles in their reduced Co(I) state. It is accepted that the catalytic cycle for hydrogen evolution proceeds via protonation of the Co(I) species, yielding a Co(III)–H hydridocobaloxime intermediate that, after further reduction to the Co(II)–H state, can evolve dihydrogen through either protonation of the hydride moiety or bimolecular reductive elimination [1, 2, 3, 4, 5, 10, 11, 6, 13, 14, 15, 16, 17, 18].

Recent reports from the groups of Muckerman [19], Hammes-Schiffer [20] and Jiang [21] have addressed aspects of the catalytic activity of these compounds using quantum chemical approaches and confirm the role of the Co(I) species. Experimentally, the spectroscopic signatures of Co(I) intermediates have been observed during the course of electro- and photo-catalytic experiments [4, 5, 22], and the Co(I) species [14, 23, 24, 9], and its protonated Co(III)-H form [25, 26, 27], have been isolated and characterized in a few, rare cases. In this context, we recently examined the sole hydridocobaloxime isolated to date, $[HCo(dmgH)_2(PnBu_3)]$ [26], using a mixture of experiment and theory [25]. The current article follows up this latter study by focusing on a deeper understanding of the electronic state of the reduced Co(I) form of the cobaloxime catalysts. For this purpose we have chosen two previously characterized Co(I)-oxime complexes — $[Na][Co(dmgH)_2(PnBu_3)]$ [25] and $[Na][Co(dmgBF_2)_2(CH_3CN)]$ [14] — which we denote compounds 1 and 2, respectively (see Figure 1). We have employed both time-dependent density functional theory (TDDFT) and correlated molecular orbital methods to characterize the electronic excitation spectra of these compounds and show that a reasonable qualitative description of them can be obtained.

3 Methods

3.1 Calculations

The ORCA [28] program (version 2.9) was employed for all DFT and TDDFT calculations. Geometry optimizations were performed at the DFT level using the BP86 [29, 30] and B3LYP [31, 32] functionals. Test calculations were also carried out with the addition of empirical van der Waals corrections [33] on compound 2 but the effects were found to be small and so will not be considered further here. To be precise, the relative ordering of the energies of the different isomers remained unchanged and the RMS heavy atom coordinate differences between equivalent optimized structures was, at most, 0.05 Å.

All geometry optimizations were done with the Ahlrichs TZVP basis sets (ORCA option ACC-OPT), which are of triple-ζ quality [34]. These were followed with single point energy and TDDFT calculations after optimization with a basis set of TZVP quality but augmented with extra polarization and diffuse functions (ORCA option DFT-ENERGY+). The combination of the BP86 functional, in particular, and a triple-ζ basis set has been shown to perform well for systems similar to the ones that we are studying, including the ground and excited states of cobalt corrinoids [35, 36].

Europe PMC Funders Author Manuscripts

In addition to DFT calculations, we also carried out single-point energy and spectra computations using higher-level *ab initio* multireference molecular orbital methods. All methods we tried were based on CASSCF wavefunctions, which in themselves are inadequate for describing dynamic correlation. However, these can be supplemented by the application of perturbative corrections or of multireference configuration interaction (MRCI). We did both by employing the CASPT2 [37] and NEVPT2 [38] perturbative methods, and the spectroscopy-oriented CI (SORCI) method developed by Neese *et al.* [39]. The CASSCF/NEVPT2 and SORCI calculations were performed using ORCA, whereas the CASSCF/CASPT2 computations were carried out with the MOLCAS [40, 41] program (version 7.4). All the calculations at this level were effected using the DFT optimized geometries obtained previously. For the results that we report in this paper, the basis sets that were employed were as follows: CASPT2 — both the ANO-L-VDZP and ANO-L-VTZP bases [42]; NEVPT2 — a composite basis consisting of an Ahlrich's TZVP basis for the metal, the four equatorial coordinating nitrogens and, where applicable, the phosphorus, but with an Ahlrichs split valence with polarization (SVP) basis for all other atoms; SORCI — an SVP basis for all atoms. We would have preferred to use full TZVP bases for the NEVPT2 and SORCI calculations but were unable to obtain a complete set of converged results with this larger basis (see section 4.3 for a fuller discussion).

All calculations, both DFT and *ab initio*, were done in an implicit solvent model of acetonitrile, using the COSMO [43] and PCM [44, 45] methods implemented in ORCA and in MOLCAS, respectively.

3.2 Experiments

$[Co(dmgBF_2)_2(CH_3CN)_2]$ was prepared according to the method of Bakac and Espenson [46]. $[Na][Co(dmgBF_2)_2(CH_3CN)]$ was prepared by reaction of $[Co(dmgBF_2)_2(CH_3CN)_2]$ with excess sodium mercury amalgam (0.5% Na) under vacuum in anhydrous acetonitrile, analogous to a literature preparation for the diphenyl-glyoximato analogue [47]. The solution of the partially reduced species was transferred over a frit to a fused 2-mm quartz cuvette; the reduction process was monitored via UV-vis absorption spectroscopy (Hewlett-Packard 8452 spectrophotometer) until the reduction was complete.

4 Results

4.1 Geometries

Summaries of pertinent bond distances and angles in the optimized DFT structures of compounds 1 and 2 are given in Table 1. Preliminary calculations (data not shown) indicated that both functionals strongly favored penta-coordination for the cobalt, leaving one axial position unoccupied, and that the singlet state of the compounds was the one that was energetically preferred. The B3LYP functional favored smaller, although still significant, energy gaps to the higher spin states (~ 50 kJ mol^{-1}) than BP86 (~ 125 kJ mol^{-1}).

A feature of the coordination around cobalt in compound 2 is that each of its BF_2 groups can adopt two orientations relative to the plane containing the cobalt and its four coordinating equatorial nitrogens. We denote these possibilities as *d* or *u* if a BF_2 points away from or

towards the coordinating axial acetonitrile, respectively. This gives three different isomers which are labelled as *dd*, *du* and *uu* in Table 1. We note that previous theoretical work on these compounds seem to have considered only the *du* isomer [19, 20]. With each functional, we find that the *dd* isomer is the most stable, followed by *du* and then *uu*. However, the energy differences are very small being only 1 kJ mol^{-1} between the *dd* and *uu* isomers with B3LYP and 4 kJ mol^{-1} with BP86.

Structurally the two functionals give similar complexes with the most significant differences occurring between the cobalt and the atoms to which it is bound. Overall it can be seen that BP86 favors shorter bond distances to cobalt than B3LYP, and that it favors a more nearly four-fold symmetrical coordination environment in compound 2 as the equatorial Co–N bond distances are almost equal and the Co–N–C (MeCN) bond angles are almost straight. We note that the compound 2 geometries are, to a very good approximation, of C_s symmetry, whereas those of compound 1 belong to the C_1 point group.

4.2 Experimental and DFT spectra

The experimental and calculated TDDFT UV spectra, both obtained in acetonitrile, are shown for compounds 1 and 2 in the top panels of Figure 2 and the values of the absorption bands in Table 2.

Experimentally compound 1 has a single dominant absorption maximum at 606 nm within the 400–750 nm wavelength window. The absorption at shorter wavelengths is significant with a shoulder at ~520 nm and an increase in absorption towards 400 nm. By contrast, compound 2 has two dominant maxima, at 553 and 628 nm, with the former being slightly more intense, and the absorption decreases markedly at shorter wavelengths [14].

The calculated BP86 and B3LYP TDDFT spectra for compound 1 both show single dominant bands within the 400–750 nm wavelength range but they occur at wavelengths that are too short (by 97 and 71 nm, respectively) with respect to the experimental band. At shorter wavelengths, the B3LYP spectrum has significant absorption but that of the BP86 spectrum decays rapidly to zero, unlike experiment.

The calculated TDDFT spectra for compound 2 show more structure. The BP86 spectra for each isomer show two dominant bands, like experiment, but they are again shifted to shorter wavelengths (~ 80–100 nm), and the longer wavelength band is more intense. By contrast, the B3LYP spectra have three bands, at approximately 100 nm intervals, that increase in oscillator strength on going to shorter wavelengths. The two longest wavelength bands are also shifted to shorter wavelengths compared to experiment but less markedly so, by ~ 20–40 nm, than those of BP86. We note that the B3LYP spectrum of compound 2 is very similar to that obtained by Muckerman and Fujita for the *du* isomer [19].

4.3 Ab initio spectra

In principle, *ab initio* methods provide a systematically improvable route to the calculation of electronic properties. For transition metal compounds, a reasonable starting point for the calculation of electronic spectra is the use of a correlated CASSCF method [48]. The problem here is that the computational and memory requirements of these calculations for

Europe PMC Funders Author Manuscripts

molecules as large as compounds 1 and 2 (~ 70 atoms), with reasonably sized active spaces, are extremely challenging, even with the most powerful desktop workstations. To overcome this in the present case, we employed truncated models for these compounds (see Figure 1), in which the methyl groups of the rings in both compounds have been replaced by hydrogens, and the *n*-butyl groups in compound 2 have been replaced by methyls.

Caution must be taken during the structural optimization of these truncated models, as we have found that full optimization can bring about considerable change in the metal coordination environment. This is especially so for compound 1 as truncation of the large *n*-butyl groups attached to the phosphine ligand has an important influence on the geometry about the cobalt atom. Therefore, as an alternative strategy, we took the geometry-optimized structures of the full compounds and only optimized the hydrogen atom positions. As an aside we note that we enforced C_s symmetry on the truncated compound 2 structures. For the BP86 and B3LYP *uu* optimized structures, this required adjustments of the heavy atom coordinates of less than 0.01 Å as the structures were already very nearly symmetric. For the *dd* and *du* B3LYP optimized structures, the adjustments were somewhat greater as the CCH_3 portion of the axial acetonitrile ligands did not lie in the symmetry plane and so needed to be rotated (by ~ 15 and 5°, respectively). Nevertheless, we note that the final optimized energy differences between the symmetrized and unsymmetrized pairs of structures were always within 1 kJ mol^{-1}, and that the symmetric forms were often the more stable.

TDDFT calculations of the spectra of these partially-optimized truncated models show that the effect on the excitation energies is quite small (see the top panels of Figure 2). In all cases, the bands in the truncated models are shifted to slightly shorter wavelengths with the maximum shifts being 6, 10, 11 and 15 nm for the compound 1 B3LYP and BP86, and compound 2 B3LYP and BP86 spectra, respectively. These differences are minor given the error inherent in the quantum chemical description, and the fact that it permits the application of higher level of theories. These observations are in agreement with the results of other workers who have employed similar strategies [35].

For our multireference calculations we employed the ORCA and MOLCAS programs, the former for its CASSCF/NEVPT2 and SORCI methods, and the latter for its CASSCF/CASPT2 approach. We found MOLCAS to be much more robust for CASSCF computations than ORCA. In particular, the CASSCF procedure always progressed smoothly with MOLCAS, whereas convergence was troublesome, and often impossible, with ORCA, especially with the larger active spaces. Calculations with both programs were computationally very demanding at these levels of theory, even for the truncated models, and so we have certainly not been able to achieve converged results, either in terms of basis set or the size of the active space. Nevertheless, the results we obtained are consistent with those of the TDDFT calculations and give qualitative insights into the nature of the low-energy electronic absorption bands for these compounds. Exploratory calculations with ORCA showed that the B3LYP optimized geometries consistently had the lowest energies with the *ab initio* methods (by ~ 50 kJ mol^{-1}) and so we consider only these in what follows.

The choice of active space is crucial when performing CASSCF calculations and involves both chemical intuition and much trial and error. Systematic routes to active space selection,

such as identifying orbitals with partial occupancies from DFT and MP2 calculations, tend to give spaces that are too large for feasible calculation [48]. Overall, the calculations we consider most reliable were obtained using the CASSCF/CASPT2 method in MOLCAS with an active space consisting of 12 electrons in 14 active orbitals, which we denote CAS(12,14). This was designed to include the five cobalt 3d occupied orbitals and an extra d-shell to account for the 3d double-shell effect. The highest occupied and a correlating lowest unoccupied ligand molecular orbital per irreducible representation were also included, giving a total of 4 (as compound 2 has C_s symmetry and so two irreducible representations), to allow for possible LMCT and MLCT excitations. The 3d double-shell correlation effect occurs in firstrow transition metals with more than half filled 3d shells because these atoms have a relatively dense 3d shell due to a large number of electrons located in a contracted spatial distribution [49].

The CASSCF and CASPT2 calculations [37] were performed in vacuum and PCM implicit solvent with ANO-L-VDZP and ANO-L-VTZP basis sets [42]. The results were actually very similar for all four combinations of environment and basis set with differences of a maximum of 6 nm in the wavelengths of the dominant bands for the two calculations in solvent and a slightly larger 10 nm between those in solvent and in vacuum. The values that we show in Figure 2 and Tables 2 and 3 are those obtained with the ANO-L-VDZP basis in an acetonitrile implicit solvent. Compound 1 had C_1 symmetry and its lowest 15 roots were state-averaged with equal weights. Compound 2 had C_s symmetry and its basis was symmetry-adapted. State-averaged CASSCF calculations were performed including the lowest 5 and 10 roots with equal weights for the A′ and A″ irreducible representations. In the CASPT2 calculations, the external part of the zero order Hamiltonian was shifted by 0.3 atomic units to eliminate contributions from intruder states. All valence electrons were correlated, excluding the cobalt 3s electrons. For calculations performed in PCM solvent, reaction field effects were added in the one-electron Hamiltonian in the CASPT2 calculation. Non-equilibrium solvation effects were also included in the excited state CASSCF calculations. Finally, oscillator strengths were obtained by performing state interaction calculations from the CASSCF wavefunctions.

The CASPT2 spectra are shown for compounds 1 and 2 in the middle panels of Figure 2 and the values of the absorption bands in Table 2. From the figures it appears that the CASPT2 spectra have the same qualitative features as the experimental data but that the peaks are shifted in a systematic manner. A linear-least squares fit between the experimental and calculated data, in energy space, gives a common adjustment parameter of −3350 cm^{-1}, which when applied to the raw CASPT2 spectra gives the shifted curves that are also shown in Figure 2 and are in much better quantitative agreement with experiment. This shift of the CASPT2 spectra in comparison to experiment is in line with the normal error bar for CASPT2 excitation energies (≈ 0.3 eV) [50].

The order of stability of the isomers of compound 2 at this level of theory, in contrast to the DFT results, is *du* < *uu* << *dd*. An analysis of the correlation energies shows that these are much more favorable for *du* and *uu* than *dd*. The exact values depend on the basis and the environment, but with the ANO-L-VTZP basis and in implicit solvent, the relative energies of the CASSCF ground states are 0, 6 and 13 kJ mol^{-1} for the *dd*, *du* and *uu* isomers,

respectively, but these change to 131, 0 and 2 kJ mol^{-1} when the CASPT2 corrections are included. This implies that the *dd* isomer is unpopulated and so does not contribute to the spectra shown in Figure 2.

As mentioned above, we found the MOLCAS program to be more robust when performing the higher level calculations. Nevertheless, we were able to obtain some data using ORCA, two examples of which we show in the bottom panels of Figure 2 and in Table 2. The perturbative approach that ORCA implements is a strongly contracted version of NEVPT2, which has the advantage over CASPT2 of being free from intruder states [38]. We show results for NEVPT2 applied to the largest state-averaged CASSCF wavefunction that we were able to obtain with ORCA, namely 14 electrons in 11 active orbitals, consisting of 5 Co d orbitals and 6 predominantly ligand orbitals. In each case 10 roots were calculated with, for compound 2, 5 roots each of the A′ and A″ irreducible representations.

The CAS(14,11)/NEVPT2 spectrum for compound 1 is actually in very good quantitative agreement with experiment at longer wavelengths although in common with the B3LYP spectrum for the truncated model it lacks the absorptions at shorter wavelengths. By contrast, the CAS(14,11)/NEVPT2 spectrum for compound 2 resembles closely the CAS(12,14)/CASPT2 spectrum, with an equivalent shift with respect to experiment, but with an inversion in the oscillator strengths of the two strongest bands. For comparison, we note that a CAS(12,9) space gave spectra for the compound 2 isomers with the same dominant bands but at wavelengths shorter by between 7 and 13 nm. By contrast, the CAS(12,9)/NEVPT2 spectrum of compound 1 also had a single dominant band, like its CAS(14,11) counterpart, but shifted to a higher wavelength by 43 nm.

The second set of *ab initio* results that we obtained with ORCA are for SORCI calculations based upon CASSCF wavefunctions with CAS(8,7) and CAS(10,7) spaces for compounds 1 and 2, respectively. We present these for illustrative purposes only as we think that this is a very promising technique but do not feel that we were able to employ large enough active spaces, nor compute sufficient CI roots (due to the expense of the computations), to draw definitive conclusions.

4.4 Analysis of the absorption bands

Examination of the low-energy absorption bands of the calculated spectra show that they are dominated by MLCT but with some contributions from metal intravalence orbital transitions (MIVT). The presence of low-energy transitions involving ligand orbitals implies that the ligands are potentially redox active as we have observed in previous work [25]. In the remainder of this section, we treat the CAS(12,14)/CASPT2 spectra as reference and then contrast them with the spectra determined using the other approaches. An analysis of the configurations that contribute to the CASPT2 absorption bands is given in Table 3. Note that the 4d active space orbitals that were included to account for the double shell effect are omitted as they have zero occupancy for all the configurations that we discuss in this section. For illustration, we also show in Figure 3 the active space orbitals for the truncated model compounds that make the largest contributions to the low-energy transitions.

Analysis of the compound 1 calculations indicates that the ground state is essentially a single configuration with the active space orbital configurations shown in Table 3. The most intense absorption, at 511 nm, is of MLCT-type with major and minor contributions from (3xz) → L and ($3z^2$) → L single excitations, respectively. The second most intense band, at 383 nm, is dominated by an internal single excitation between the cobalt's ($3z^2$) and (3xy) orbitals. Finally, the third band, at 338 nm, is primarily a mixture of double excitations between ligand and cobalt 3d orbitals.

The nature of the three main bands in the B3LYP spectrum for the full model of compound 1 (see Table 2) resembles very closely the CASPT2 results — namely two MLCT transitions with an intervening transition primarily of MIVT type. By contrast, in the remaining compound 1 spectra — BP86, NEVPT2 and SORCI — MIVT is much less significant and all bands are dominanted by transitions of type MLCT.

The CASPT2 wavefunction of compound 2 has a more complicated structure than that of compound 1. The active space in these calculations consists of 8 and 6 orbitals of symmetry character a′ and a″, respectively, of which only 5 a′ and 4 a″ orbitals are shown in Table 3 as the 4d orbitals have zero occupancy and are omitted. The ground states of the three isomers in both vacuum and implicit solvent, and for both basis sets, display a pronounced multiconfigurational character. They all have a main configuration with a weight of ~ 65% that is shown in Table 3, but there are also several di-radical contributions with weights of ≤ 15% in the total wavefunction.

In the CASPT2 spectra for all three isomers of compound 2, the two highest oscillator strength excitations were of type MLCT $3x^2$-y^2 (long wavelength) and MLCT 3xz (short wavelength) with minor contributions from MIVT $3z^2$/3xy → 3yz. This contrasts to the spectrum of compound 1 for which excitations of the latter two types were significant but MLCT $3x^2$-y^2 transitions were not observed.

Unlike compound 1, the absorption bands in the compound 2 spectra obtained with the other methods all share the same MLCT and MIVT features between equivalent orbitals, with the exception of the SORCI spectrum for which MLCT bands dominate. In the B3LYP compound 2 spectra, there are three principal peaks, which correspond to MLCT, MIVT and MLCT transitions, respectively. By contrast, in the BP86 spectra, there are two peaks with the longer wavelength corresponding to the MLCT $3x^2$-y^2 transition and the shorter wavelength peak being a mixture of MLCT 3xz and MIVT 3xy→ 3yz character. Likewise, in the NEVPT2 spectra, the shorter wavelength bands involve combinations of MLCT and MIVT transitions.

5 Conclusions

In this work we have investigated the low energy electronic absorptions of two cobaloxime systems that show promise as molecular bio-inspired catalysts for hydrogen evolution. Being able to reliably predict the electronic structure and transitions of these compounds, via calculation, is essential for elucidating their mechanisms of hydrogen evolution and for designing improved catalysts. We have studied the performance of both TDDFT and *ab*

initio methods, using full structural models for the TDDFT calculations and truncated models for the more computationally intensive *ab initio* techniques. Overall, we find reasonable qualitative agreement between experiment and the spectra obtained using the different theoretical approaches, with the dominant contributions to the absorption bands coming from MLCT between the cobalt d-orbitals and the equatorial ligands, with transitions within the metal's valence orbitals playing a less important role. A quantitative reproduction of the experimental spectra, however, remains a task for future work.

Acknowledgement

Financial support from the French National Research Agency (NiFe-Cat, ANR-10-BLAN-7-11 and LABEX ARCANE, ANR-11-LABX-0D03-01), the FP7 CEA-Eurotalent COFUND Programme, the CEA's DSV-ENERGIE 2011 Programme, the European Research Council under the European Union's Seventh Framework Programme (FP/2007-2013)/ERC Grant Agreement no. 306398, the NSF Center for Chemical Innovation (CCI Solar, CHE-1305124), the U.S. Department of Energy (DOE) under contract number DE-AC02-98CH10886, and the Brazilian FAPESP (project 12/02501-4) is gratefully acknowledged.

References

[1]. Razavet M, Artero V, Fontecave M. Proton electroreduction catalyzed by cobaloximes: Functional models for hydrogenases. Inorg. Chem. 2005; 44:4786–4795. [PubMed: 15962987]

[2]. Hu X, Cossairt BM, Brunschwig BS, Lewis NS, Peters JC. Electrocatalytic hydrogen evolution by cobalt difluoroboryl-diglyoximate complexes. Chem. Commun. 2005; 41:4723–4725.

[3]. Baffert C, Artero V, Fontecave M. Cobaloximes as functional models for hydrogenases. 2. Proton electroreduction catalyzed by difluoroborylbis(dimethylglyoximato) cobalt (II) complexes in organic media. Inorg. Chem. 2007; 46:1817–1824. [PubMed: 17269760]

[4]. Hu X, Brunschwig BS, Peters JC. Electrocatalytic hydrogen evolution at low overpotentials by cobalt macrocyclic glyoxime and tetraimine complexes. J. Am. Chem. Soc. 2007; 129:8988–8998. [PubMed: 17602556]

[5]. Pantani O, Anxolabehere-Mallart E, Aukauloo A, Millet P. Electroactivity of cobalt and nickel glyoximes with regard to the electro-reduction of protons into molecular hydrogen in acidic media. Electrochem. Commun. 2007; 9:54–58.

[6]. Jacques PA, Artero V, Pécaut J, Fontecave M. Cobalt and nickel diimine-dioxime complexes as molecular electrocatalysts for hydrogen evolution with low overvoltages. Proc. Natl. Acad. Sci. 2009; 106:20627–20632. [PubMed: 19948953]

[7]. Andreiadis ES, Jacques P-A, Tran PD, Leyris A, Chavarot-Kerlidou B, Jousselme M, Matheron M, Pécaut J, Palacin S, Fontecave M, Artero V. Molecular engineering of a cobalt-based electrocatalytic nano-material for H_2 evolution under fully aqueous conditions. Nat. Chem. 2013; 5:48–53. [PubMed: 23247177]

[8]. Bhattacharjee A, Andreiadis ES, Chavarot-Kerlidou M, Fontecave M, Field MJ, Artero V. A computational study of the mechanism of hydrogen evolution by cobalt(diimine-dioxime) catalysts. Chemistry — A European Journal. 2013; 19:15166–15174.

[9]. Zhang P, Jacques PA, Chavarot-Kerlidou M, Wang M, Sun L, Fontecave M, Artero V. Phosphine coordination to a cobalt diimine–dioxime catalyst increases stability during light-driven H_2 production. Inorg. Chem. 2012; 51:2115–2120. [PubMed: 22313315]

[10]. Artero V, Chavarot-Kerlidou M, Fontecave M. Splitting water with cobalt. Angew. Chem. Int. Ed. 2011; 50:7238–7266.

[11]. Dempsey JL, Brunschwig BS, Winkler JR, Gray HB. Hydrogen evolution catalyzed by cobaloximes. Acc. Chem. Res. 2009; 42:1995–2004. [PubMed: 19928840]

[12]. Dempsey JL, Winkler JR, Gray HB. Solar fuels: approaches to catalytic hydrogen evolution. Comprehensive Inorganic Chemistry II: From Elements to Applications. 2013; 8:553–565.

[13]. Dempsey JL, Winkler JR, Gray HB. Kinetics of electron transfer reactions of H_2-evolving cobalt diglyoxime catalysts. J. Am. Chem. Soc. 2009; 132:1060–1065. [PubMed: 20043639]

[14]. Dempsey JL, Winkler JR, Gray HB. Mechanism of H_2 evolution from a photogenerated hydridocobaloxime. J. Am. Chem. Soc. 2010; 132:16774–1677. [PubMed: 21067158]

[15]. Du P, Schneider J, Luo G, Brennessel WW, Eisenberg R. Visible light-driven hydrogen production from aqueous protons catalyzed by molecular cobaloxime catalysts. Inorg. Chem. 2009; 48:4952–4962. [PubMed: 19397296]

[16]. Du P, Knowles K, Eisenberg R. A homogeneous system for the photogeneration of hydrogen from water based on a platinum (II) terpyridyl acetylide chromophore and a molecular cobalt catalyst. J. Am. Chem. Soc. 2008; 130:12576–12577. [PubMed: 18759395]

[17]. Lazarides T, McCormick T, Du P, Luo G, Lindley B, Eisenberg R. Making hydrogen from water using a homogeneous system without noble metals. J. Am. Chem. Soc. 2009; 131:9192–9194. [PubMed: 19566094]

[18]. McCormick TM, Calitree BD, Orchard A, Kraut ND, Bright FV, Detty MR, Eisenberg R. Reductive side of water splitting in artificial photosynthesis: New homogeneous photosystems of great activity and mechanistic insight. J. Am. Chem. Soc. 2010; 132:15480–15483. [PubMed: 20945839]

[19]. Muckerman JT, Fujita E. Theoretical studies of the mechanism of catalytic hydrogen production by a cobaloxime. Chem. Commun. 2011; 47:12456–12458.

[20]. Solis BH, Hammes-Schiffer S. Theoretical analysis of mechanistic pathways for hydrogen evolution catalyzed by cobaloximes. Inorg. Chem. 2011; 50:11252–11262. [PubMed: 21942543]

[21]. Jiang YK, Liu JH. DFT studies of cobalt hydride intermediate on cobaloxime-catalyzed H_2 evolution pathways. Int J. Quantum Chem. 2012; 112:2541–2546.

[22]. Du P, Schneider J, Luo G, Brennessel WW, Eisenberg R. Visible light-driven hydrogen production from aqueous protons catalyzed by molecular cobaloxime catalysts. Inorg. Chem. 2009; 48:4952–4962. [PubMed: 19397296]

[23]. Costa G, Mestroni G, De Savorgnani E. Vitamin B_{12} model compounds-cobalt chelates of bis (diacetylmonoxime-imino) propane 1–3. Inorg. Chim. Acta. 1969; 3:323–328.

[24]. Weakley TJR, Marks J, Finke RG. The cobalt (I) coenzyme B_{12} model complex [2, 10-diethyl-3, 9-dimethyl-1, 4, 8, 11-tetraazaundeca-1, 3, 8, 10-tetraene-1, 11-diolato (1-)](triphenylphosphine) cobalt (I). Acta Cryst. C. 1994; 50:1690–1692.

[25]. Bhattacharjee A, Chavarot-Kerlidou M, Andreiadis ES, Fontecave M, Field MJ, Artero V. Combined experimental and theoretical characterization of the hydrido-cobaloxime $[HCo(dmgH)_2(PnBu_3)]$. Inorg. Chem. 2012; 51:7087–7093. [PubMed: 22712692]

[26]. Schrauzer GN, Holland RJ. Hydridocobaloximes. J. Am. Chem. Soc. 1971; 93:1505–1506.

[27]. Li G, Pulling ME, Estes DP, Norton JR. Cobaloxime-mediated radical cyclization under H_2. Evidence for formation of a Co-H bond and kinetics of $H^{\bullet}$ transfer. J. Am. Chem. Soc. 2012; 134:14662–14665. [PubMed: 22897586]

[28]. Neese F. The ORCA program system. WIREs Comput Mol Sci. 2012; 2:73–78.

[29]. Becke AD. Density-functional thermochemistry. III. The role of exact exchange. Chem. Phys. 1993; 98:5648–5652.

[30]. Perdew JP. Density-functional approximation for the correlation energy of the inhomogeneous electron gas. Phys. Rev. B. 1986; 33:8822–8824.

[31]. Becke AD. Density-functional exchange-energy approximation with correct asymptotic behavior. Phys. Rev. B. 1988; 38:3098–3100.

[32]. Lee C, Yang W, Parr RG. Development of the Colle-Salvetti correlation-energy formula into a functional of the electron density. Phys. Rev. B. 1988; 37:785–789.

[33]. Schwabe T, Grimme S. Towards chemical accuracy for the thermodynamics of large molecules: new hybrid density functionals including nonlocal correlation effects. Phys. Chem. Chem. Phys. 2006; 8:4398–4401. [PubMed: 17001405]

[34]. Weigend F, Ahlrichs R. Balanced basis sets of split valence, triple zeta valence and quadruple zeta valence quality for H to Rn: Design and assessment of accuracy. Phys. Chem. Chem. Phys. 2005; 7:3297–3305. [PubMed: 16240044]

[35]. Kornobis K, Kumar N, Wong BM, Lodowski P, Jaworska M, Andruniów T, Ruud K, Kozlowski PM. Electronically excited states of vitamin B_{12}: Benchmark calculations including time-

dependent density functional theory and correlated ab initio methods. J. Phys. Chem. A. 2011; 115:1280–1292. [PubMed: 21280654]

[36]. Andruniów T, Jaworska M, Lodowski P, Zgierski MZ, Dreos R, Randaccio L, Kozlowski PM. Time-dependent density functional theory study of cobalt corrinoids: Electronically excited states of coenzyme B_{12}. J. Chem. Phys. 2009; 131:105105.

[37]. Andersson K, Malmqvist PÅ, Roos BO. Second-order perturbation theory with a complete active space self-consistent field reference function. J. Chem. Phys. 1992; 96:1218–1226.

[38]. Angeli C, Cimiraglia R, Evangelisti S, Leininger T, Malrieu JP. Introduction of n-electron valence states for multireference perturbation theory. J. Chem. Phys. 2001; 114:10252–10264.

[39]. Neese F. A spectroscopy oriented configuration interaction procedure. J. Chem. Phys. 2003; 119:9428–9443.

[40]. Karlstrom G, Lindh R, Malmqvist P-Å, Roos BO, Ryde U, Veryazov V, Widmark P-O, Cossi M, Schimmelpfennig B, Neogrady P, Seijo L. MOLCAS: a program package for computational chemistry. Comput. Mat. Sci. 2003; 28:222–239.

[41]. Aquilante F, De Vico L, Ferré N, Ghigo G, Malmqvist P-Å, Neogrády P, Pedersen TB, Pitonak M, Reiher M, Roos BO, Serrano-Andrés L, Urban M, Veryazov V, Lindh R. MOLCAS 7: The next generation. J. Comput. Chem. 2010; 31:224–247. [PubMed: 19499541]

[42]. Roos BO, Lindh R, Malmqvist P-A, Veryazov V, Widmark P-O. New relativistic ANO basis sets for transition metal atoms. J. Phys. Chem. A. 2005; 109:6575–6579. [PubMed: 16834004]

[43]. Sinnecker S, Rajendran A, Klamt A, Diedenhofen M, Neese F. Calculation of solvent shifts on electronic g-tensors with the conductor-like screening model (COSMO) and its self-consistent generalization to real solvents (COSMO-RS). J. Phys. Chem. A. 2006; 110:2235–2245. [PubMed: 16466261]

[44]. Barone V, Cossi M. Quantum calculation of molecular energies and energy gradients in solution by a conductor solvent model. J. Phys. Chem. A. 1998; 102:1995–2001.

[45]. Cossi M, Rega N, Scalmani G, Barone V. Polarizable dielectric model of solvation with inclusion of charge penetration effects. J. Chem. Phys. 2001; 114:5691–5701.

[46]. Bakac A, Espenson JH. Unimolecular and bimolecular homolytic reactions of organochromium and organocobalt complexes. Kinetics and equilibria. J. Am. Chem. Soc. 1984; 106:5197–5202.

[47]. Hu X, Brunschwig BS, Peters JC. Electrocatalytic hydrogen evolution at low overpotentials by cobalt macrocyclic glyoxime and tetraimine complexes. J. Am. Chem. Soc. 2007; 129:8988–8998. [PubMed: 17602556]

[48]. Veryazov V, Malmqvist PC, Roos BO. How to select active space for multiconfigurational quantum chemistry? Int J. Quantum Chem. 2011; 111:3329–3338.

[49]. Pierloot, K. Nondynamic correlation effects in transition metal coordination compounds. In: Cundari, TR., editor. Computational Organometallic Chemistry. 1st edition. Marcel Dekker; New York: 2001. p. 123-158.

[50]. Roos BO, Andersson K, Fülscher MP, Serrano-Andrés L, Pierloot K, Merchan M, Molina V. Applications of level shift corrected perturbation theory in electronic spectroscopy. J. Mol. Struct. Theochem. 1996; 388:257–276.

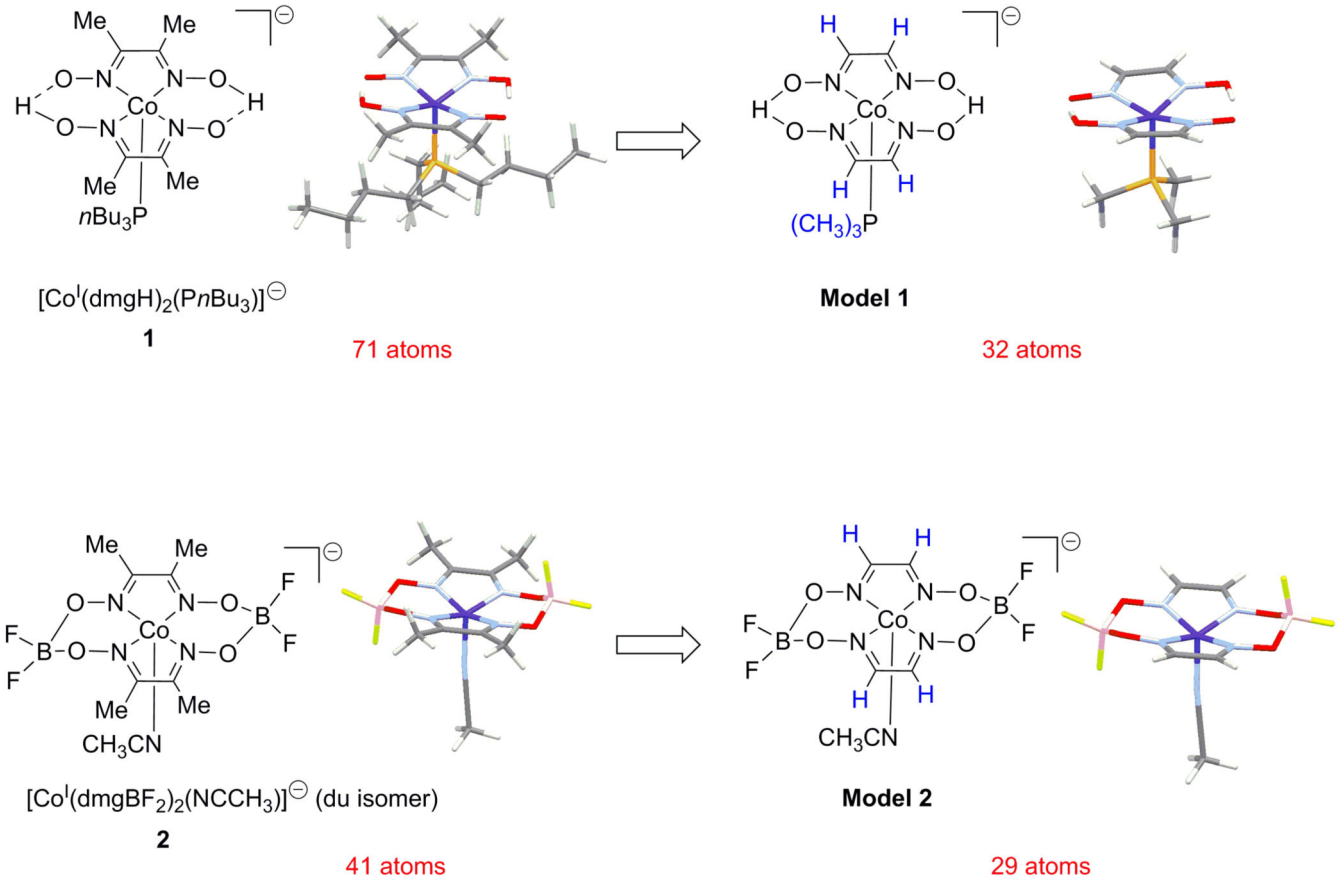

Figure 1.

Compounds 1 and 2 together with their truncated models. The *du* isomers of compound 2 are shown, with the left-hand BF_2 groups in their *u* positions and the right-hand groups in their *d* positions (note that *d* and *u* refer to orientations away from or toward the axial ligand, respectively).

Europe PMC Funders Author Manuscripts

Europe PMC Funders Author Manuscripts

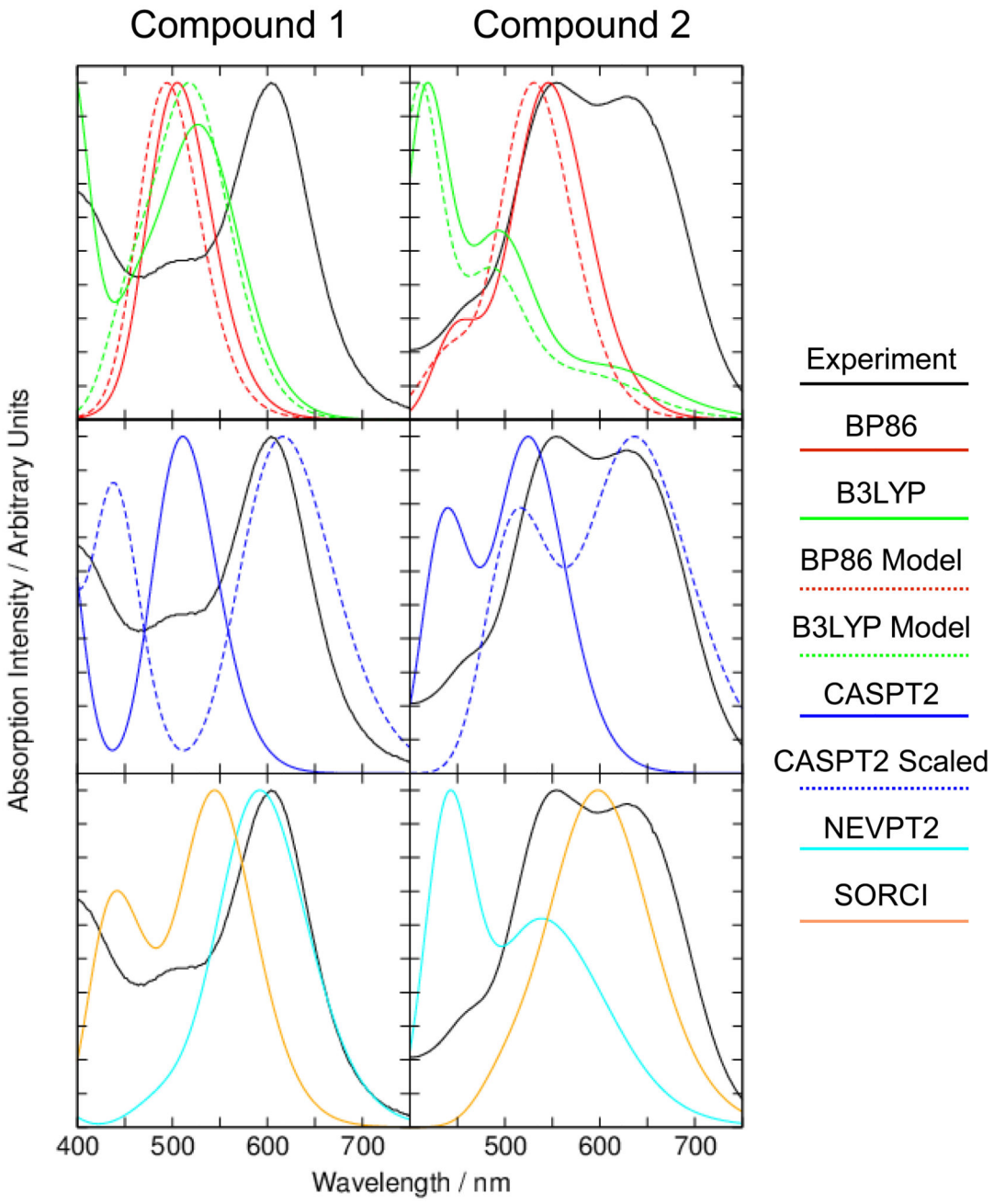

Figure 2.

Experimental and calculated spectra for compound 1 (left panels) and compound 2 (right panels). Calculations in the middle and bottom panels were done on the truncated models at their B3LYP optimized geometries. All simulated spectra were fitted using Gaussian line shapes with FWHM of 3000 cm^{-1}. The spectra of compound 2 were determined as a Boltzmann weighted average at 300 K of the spectra of its three isomers.

Europe PMC Funders Author Manuscripts

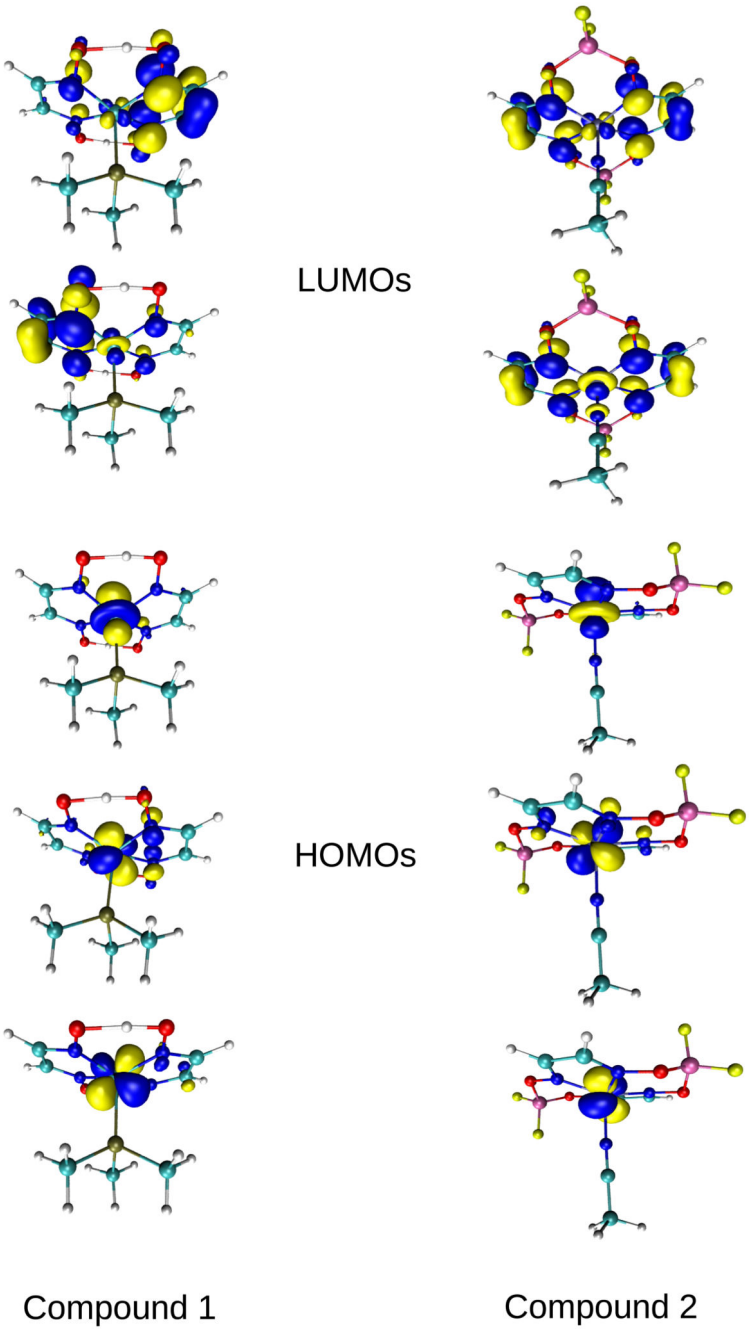

Figure 3.

Active space orbitals for the truncated models of compounds 1 (left column) and 2 (right column). Only those orbitals that make the largest contribution to the dominant absorption bands in the spectra are shown. The HOMO (bottom three) and LUMO (top two) notation refers to the occupancies of the orbitals in the nominal doubly-occupied ground state configuration. The orbitals were obtained from NEVPT2 calculations but they are typical of what are found with the other methods.

Europe PMC Funders Author Manuscripts

Table 1

A comparison of important bond lengths (Å) and bond angles (°) between the BP86 and B3LYP optimized geometries for compounds 1 and 2 in acetonitrile (MeCN).

Bond Length or Angle	**BP86**			**B3LYP**		
Compound 1						
Co–P		2.233			2.312	
Co–N		1.871			1.886	
		1.874			1.888	
		1.879			1.896	
		1.882			1.897	
Compound 2	*dd*	*du*	*uu*	*dd*	*du*	*uu*
Co–N (MeCN)	1.924	1.928	1.931	2.082	2.003	2.005
N–C (MeCN)	1.164	1.163	1.162	1.148	1.149	1.148
Co–N	1.861	1.863	1.869	1.868	1.873	1.883
	1.862	1.864	1.869	1.872	1.874	1.884
	1.862	1.865	1.869	1.880	1.881	1.885
	1.862	1.866	1.869	1.883	1.883	1.889
Co–N–C (MeCN)	179.8	179.6	179.8	168.9	174.7	170.8

Europe PMC Funders Author Manuscripts

Table 2

Experimental and calculated UV-VIS absorption bands for compounds 1 and 2 in acetonitrile. The oscillator strengths of calculated bands are given in brackets after the wavelengths. All BP86 calculations were done at the BP86-optimized geometries and all other calculations at the B3LYP-optimized geometries. Only the dominant bands with wavelengths between 400 and 750 nm and with oscillator strengths larger than 10^{-2} are shown.

Method	Isomer	Band Wavelengths (nm) and Oscillator Strengths		
Compound 1				
Experiment		606		
BP86		509 (0.09)		
B3LYP		535 (0.08)	463 (0.05)	393 (0.15)
CAS(12,14)/CASPT2		511 (0.17)	383 (0.14)	338 (0.10)
CAS(14,11)/NEVPT2		595 (0.20)		
CAS(8,7)/SORCI		567 (0.16)	470 (0.05)	432 (0.09)
Compound 2				
Experiment		628	553	
BP86	*dd*	547 (0.07)	448 (0.02)	
	du	550 (0.05)	456 (0.01)	
	uu	535 (0.03)	466 (0.02)	
B3LYP	*dd*	638 (0.04)	492 (0.16)	414 (0.17)
	du	606 (0.03)	502 (0.07)	412 (0.17)
	uu	585 (0.01)	504 (0.09)	424 (0.27)
CAS(12,14)/CASPT2	*dd*	581 (0.35)	526 (0.18)	
	du		524 (0.26)	433 (0.20)
	uu	533 (0.13)	531 (0.14)	451 (0.26)
CAS(14,11)/NEVPT2	*dd*	596 (0.11)	517 (0.16)	448 (0.22)
	du	551 (0.15)	440 (0.25)	424 (0.10)
CAS(10,7)/SORCI	*du*	610 (0.02)	558 (0.07)	504 (0.04)

Europe PMC Funders Author Manuscripts

Table 3

Analysis of the main absorption bands from the CASPT2 calculations. The first line of each band gives the natural orbital occupancies, whereas the subsequent lines detail the dominant configurations and their weights. d — spin down; f_o — oscillator strength; GS — ground state; L — ligand π orbital; λ — wavelength; u — spin up. The prime subscripts indicate the symmetries of the ligand orbitals for compound 2.

λ/nm	f_o	Active Space Orbitals									Weight	Character
Compound 1												
		L	L	3yz	3z^2	3xz	3x^2-y^2	L	L	3xy		
GS		2	2	2	2	2	2	0	0	0		
511	0.17	2	2	2	1.5	1.5	2	0.5	0.5	0		MLCT
		2	2	2	2	u	2	d	0	0	0.10	3xz → L
		2	2	2	u	2	2	d	0	0	0.14	3z^2 → L
		2	2	2	2	2	u	2	0	d	0.11	3xz → L
383	0.15	2	1.5	2	1	1.5	2	0.5	0.5	1		MIVT
		2	2	2	u	2	2	0	0	d	0.18	3z^2 → 3xy
338	0.10	2	1	2	2	1.5	2	0	0.5	1		
		2	u	2	2	d	2	u	d	0	0.13	Double excitation
		2	u	2	2	d	2	0	u	d	0.14	Double excitation
Compound 2												
		L′	3z^2	3x^2-y^2	3xy	L′	L″	3xz	L″	3yz		
GS		2	2	2	2	0	2	2	0	0		
du isomer												
524	0.26	2	2	1	2	0	2	2	1	0		MLCT
		2	2	2	u	0	2	2	d	0	0.27	3xy → L″
		2	2	u	2	0	2	2	d	0	0.41	3x^2-y^2 → L″
433	0.20	2	1.5	2	2	0.5	2	1.5	0	0.5		MIVT/MLCT
		2	2	2	2	u	2	d	0	0	0.28	3xz → L′
		2	u	2	2	0	2	2	0	d	0.31	3z^2 → 3yz
uu isomer												
533	0.13	2	2	1.5	1.5	0	2	2	0.5	0.5		MIVT/MLCT
		2	2	2	u	0	2	2	0	d	0.34	3xy → 3yz
		2	2	u	2	0	2	2	d	0	0.21	3x^2-y^2 → L″
		2	u	2	2	0	2	2	d	0	0.11	3z^2 → L″
531	0.14	2	2	1	2	0	2	2	1	0		MLCT
		2	2	2	2	u	2	d	0	0	0.15	3xz → L′
		2	2	2	u	0	2	2	0	d	0.12	3xy → 3yz
		2	2	u	2	0	2	2	d	0	0.54	3x^2-y^2 → L″
451	0.26	2	2	2	2	1	2	1	0	0		MLCT
		2	2	2	2	u	2	d	0	0	0.56	3xz → L′
		2	2	2	u	0	2	2	0	d	0.11	3xy → 3yz